

Anisotropy-dependent circular polarization spectroscopy

S. B. Bayram* and R. Marhatta

Miami University, Physics Department, Oxford, Ohio 45056, USA

(Received 9 August 2007; revised manuscript received 25 June 2008; published 8 September 2008)

We have experimentally investigated the anisotropy-dependent circular polarization spectra of the ^{133}Cs $6s^2S_{1/2} \rightarrow 6p^2P_{3/2} \rightarrow 10s^2S_{1/2}$ double-resonance transition in the presence of Ar. Satisfaction of double-resonance condition, achieved by use of a two-photon two-color pulse laser excitation scheme, was monitored by measurement of the intensity of the $9p^2P_{1/2} \rightarrow 6s^2S_{1/2}$ cascade fluorescence at 361.73 nm. In the experiment anisotropies, namely, alignment and orientation in the $6p^2P_{3/2}$ level, were produced from circularly polarized light with positive helicity. Then, a circular polarization degree was measured when both lasers were circularly polarized with positive helicities, and alternately positive and negative helicities for the $6p^2P_{3/2} \rightarrow 10s^2S_{1/2}$ transition. From the measurement, we obtained the orientation-dependent depolarization cross section in the $6p^2P_{3/2}$ level due to collisions with ground-level argon atoms. A disorientation cross section value of $151(42) \text{ \AA}^2$ is reported.

DOI: [10.1103/PhysRevA.78.033403](https://doi.org/10.1103/PhysRevA.78.033403)

PACS number(s): 32.80.-t, 32.70.Cs

I. INTRODUCTION

Experimental and theoretical study of atomic collisions with neutral atoms, molecules, and ions is a key to understand the energy and charge transfer processes, depolarization cross sections, dynamical evolution of the state multipoles, and the accurate description of the intermediate levels of the collision complex [1–5]. Although the study of collision dynamics is not new, significant advances in techniques for laser cooling and trapping of atoms, molecules and ions has enormously increased the interest in this area of research [6,7]. For example, collisions involving cold Rydberg atoms [8–10] has been a great interest in many fields of research due to the interesting properties of these atoms in astrophysical and laboratory plasmas. Also, high-resolution photoassociation spectroscopy of ultracold molecules [11–16] has become an important subject to accurately determine the potential curves of these molecules in atomic and molecular physics.

The measurement of collisional depolarization cross section between an alkali metal and rare gas atom provides valuable information about the interaction between the two species such as relaxation rates of the electronic moments. Experimental investigations of collisional depolarization in $6p^2P_{3/2}$ level cesium atoms, up to now, were carried out using incoherent light sources as optical excitation [17,18]. Guiry *et al.* [17] has experimentally studied the disorientation cross section in the $6p^2P_{3/2}$ Cs atoms in collisions with argon atoms using Zeeman scanning technique at high magnetic field to decouple nuclear spin from the electronic angular momentum. However, the effect of nuclear spin on the Hanle signal may have considerable influence on the magnitude of the depolarization cross section and this effect needs to be incorporated [19]. Fricke *et al.* [18] has employed $D2$ optical pumping technique and used various models to interpret the disorientation cross section results. Theoretical disorientation cross section in the excited level cesium atom was obtained by Ref. [20].

In this work, we have experimentally studied the disorientation cross section in the ^{133}Cs $6^2P_{3/2}$ level by measuring the anisotropy-dependent circular polarization spectra as a function of Ar gas pressure using a two-photon two-color double-resonance pulse laser technique. This technique permits selective excitation in the Zeeman sublevels and direct measurement of the time evolution of the state multipoles, both of which are difficult to study by other means. Thus, it provides a wealth of information on the collisional dynamics in the excited level cesium atoms. To our knowledge, there are no experimental observations of the disorientation cross section in the cesium $6p^2P_{3/2}$ level using such a technique. Our spectra yield a direct measure of the importance of the circular polarization to the alignment- and orientation-dependent inelastic process in alkali-metal-rare-gas collisions and may provide additional insight into the collisional dynamics for the excited level alkali-metal atoms.

II. BASIC STATE MULTIPOLE CONCEPTS

In this section we provide a basic description of angular momentum polarization by considering alkali-metal atoms in $^2P_{3/2}$ levels, which can be characterized by describing the distribution of atoms over the Zeeman sublevels. Expansion of each density vector in its spherical basis provides information about the state multipole moments as described by Baylis [21]. We consider here the monopole, dipole, and quadrupole components of the total density of the $J=3/2$ atoms, and describe angular momentum polarization in the excited level in terms of these state multipole moments which contain all the dynamical information about the system. The excitation of an ensemble of atoms is done by a double-resonant absorption of two-photon two-color circularly polarized light through the $6s^2S_{1/2} \rightarrow 6p^2P_{3/2} \rightarrow 10s^2S_{1/2}$ transition.

An excited atom in a quantum state with total energy E possesses a definite angular momentum $|J|$ which is quantized in space, such that the projection of the angular momentum vector along the quantization axis is m . In an axially symmetric system, we consider an ensemble of atoms which

*bayramsb@muohio.edu

is initially in a ground state with angular momentum $1/2$, and then is excited to a state with $J=3/2$. For excitation with a linearly polarized light, the z axis can be chosen in such a way that the direction of the light electric field, defines a quantization axis for the atomic angular momentum parallel to the z axis. Thus, transitions occur between the ground and excited state magnetic sublevels with $\Delta m=0$. For excitation with circularly polarized light, the propagation direction of the light can be chosen as the quantization axis (z axis) and transitions occur between the ground and excited state magnetic sublevels with $\Delta m=+1$ or $\Delta m=-1$ depending on the light of positive or negative helicities, respectively. Since our excitation processes (pump and probe lasers) are axially symmetric with respect to the quantization axis, the excited state density matrix is diagonal with respect to the z axis. Although there are four axially symmetric multipoles with the highest rank up to $k=2J=3$ (octupole) in the $J=3/2$ level, the dipole transition can only probe the highest multipole of rank 2. Therefore, with the quantization axis parallel to the propagation direction of the light, the $J=3/2$ level can be specified by the zeroth components of multipoles of rank $k=0, 1$, and 2 . The ensemble of $J=3/2$ atoms is characterized in terms of population (monopole moment), orientation (dipole moment), and alignment (quadrupole moment). Consequently, the specific components of each tensor of rank k are determined by the polarization of the light, and by the selection of quantization axis.

When atoms with nonzero nuclear spin are studied in collisions with rare gases, the collisional relaxation rates of the electronic moments becomes complicated. Thus, density matrix methods with expansions in irreducible tensor components (also called anisotropies or state multipoles) are introduced in order to obtain explicit expressions for the angular momentum polarization [22,23]. It is important to note that coherences are not generated between Zeeman sublevels in the excited state with the quantization axis along the propagation direction of the light. Although a particular collision can generate coherences between Zeeman sublevels, these do not survive averaging over isotropic collisions with Ar atoms [24]. It should also be noted that spontaneous emission to lower levels can generate coherences, but these coherences are averaged out over the ensemble of atoms. In order to narrate the experiment and the results, it is instructive to introduce some important parameters used to describe state multipoles [22,25–28], specifically alignment and orientation involved in our experiment.

Alignment and orientation. Axially symmetric systems can be arranged by their transformation properties under a reversal of the symmetry axis. If the ensemble of atoms is invariant under the reversal of the symmetry z axis, all the values of the observables remain unchanged. This condition can only be satisfied for an axially symmetric system if it possess no net angular momentum due to the balance in the populations of the Zeeman sublevels with magnetic quantum number $\pm m$. Such a system can be described by an average tensor multipole using irreducible tensor operators of even rank. The second-rank tensor, describes the electric quadrupole polarization moment, is known as “alignment.” The alignment can be defined in terms of the angular momentum quantum numbers [22,25] as

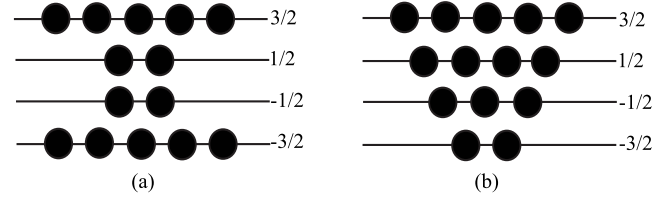


FIG. 1. Axially symmetric system showing the (a) alignment population distribution and (b) orientation population distribution over the Zeeman sublevels for the $J=3/2$ atoms.

$$\langle A_0 \rangle = \sum_m |\sigma(m)|^2 \frac{[3m^2 - J(J+1)]}{J(J+1)}, \quad (1)$$

where J is the total angular momentum of the excited level and $\sigma(m)$ is the differential cross section for excitation of the magnetic sublevels with quantum number m . Since alignment provides information on the nature of the spatial distribution of angular momentum vectors, it can be related to the shape of the excited level charge distribution.

If an axially symmetric system is not invariant under a reversal of the symmetry z axis, the symmetry is broken and system possess a net angular momentum due to the imbalance in the populations of the Zeeman sublevels. The population imbalance in the $\pm m$ sublevels can be created by absorption of circularly polarized light under the selection rule $\Delta m = \pm 1$. Thus, this condition can only be satisfied by an average tensor multipole using irreducible tensor operators of odd rank in the absence of the external magnetic field effect on the Zeeman sublevels. The first-rank tensor, describes the magnetic dipole polarization moment, is known as “orientation.” Thus, orientation can be defined in terms of the angular momentum quantum numbers [22,25] as

$$\langle O_0 \rangle = \sum_m |\sigma(m)|^2 \frac{m}{\sqrt{J(J+1)}}. \quad (2)$$

Using the analogy of Greene and Zare [25], the population distribution among the magnetic sublevels for an aligned and an oriented level for the $J=3/2$ atoms are illustrated in Figs. 1(a) and 1(b), respectively. In the $|Jm\rangle$ representation, the levels $|J \pm m\rangle$ are equally populated and thus the aligned system possesses no net angular momentum and no preferred spin direction. In the same representation, the levels $|J \pm m\rangle$ are not equally populated and thus the oriented system possesses a net angular momentum. The spatial distribution of angular momenta in the alkali-metal ${}^2P_{3/2}$ level can be purely aligned by a linearly polarized light which equally populates the $m = \pm 3/2$ levels under the selection rule $\Delta m=0$. However, one can have both alignment and orientation in the ${}^2P_{3/2}$ level with an excitation of circularly polarized light (as in the case of this work).

III. CIRCULAR POLARIZATION SPECTRA

Although the collision process can be generally described in the collision frame of coordinates (x, y, z) , the detection of the fluorescence is better described in a detector frame of coordinates (x', y', z') [25]. The multipole moments in the

two coordinate frames are related with the Euler angles (ϕ, θ, χ) using rotation matrices. In our experiment, it is not necessary to rotate the collision frame of coordinates into the detector frame of coordinates since the detector and collision frames share a common z axis. Thus, only axially symmetric tensors with the zeroth components can be nonzero in the cylindrically symmetric collision frame. The angle χ describes the orientation of a polarization analyzer while θ and ϕ describe the spatial orientation of the detector. The azimuthal angle ϕ is irrelevant in the study of a cylindrically symmetric collision frame. We choose the axis of the detector along the z' direction and a quantization axis (z axis) along the propagation directions of the pump and probe lasers. The intensity of the fluorescence radiation can be written as a function of Euler angles as [25]

$$I(\theta, \chi) = \frac{I_0}{3} \left\{ 1 - \frac{1}{2} h^{(2)}(JJ') \langle A_0 \rangle P_2(\cos \theta) + \frac{3}{2} h^{(1)}(JJ') \times \langle O_0 \rangle \cos \theta \sin 2\beta + \frac{3}{4} h^{(2)}(JJ') \times \langle A_0 \rangle \sin^2 \theta \cos 2\chi \cos 2\beta \right\}, \quad (3)$$

where $\beta = \pm \frac{\pi}{4}$ for circularly polarized light, $P_2(\cos \theta) = \frac{3}{2} \cos^2 \theta - \frac{1}{2}$ is the second rank Legendre polynomial, and where $h^{(1)}(JJ')$ and $h^{(2)}(JJ')$ are the geometrical factors that are derived from the reduced matrix elements of the density matrices and that depend only on the initial angular momentum (J) and final angular momentum (J') of the electronic levels involved. For the $6p^2P_{3/2} \rightarrow 10s^2S_{1/2}$ transition, $h^{(1)}(JJ')$ has a value of $\sqrt{5/3}$ and $h^{(2)}(JJ')$ has a value of $-5/4$ [25]. In our experiment, the helicity of the first laser, responsible for the $6s^2S_{1/2} \rightarrow 6p^2P_{3/2}$ transition, was kept positive while the helicity of the second laser, responsible for the $6p^2P_{3/2} \rightarrow 10s^2S_{1/2}$ transition, was alternately changed from positive to negative with respect to the helicity of the first laser. For the positive helicity of the second laser $I(\beta) = I(\pi/4)$ and for the negative helicity of the second laser $I(\beta) = I(-\pi/4)$. A general expression of a circular polarization can be written as

$$P_c = \frac{I(\beta = \pi/4) - I(\beta = -\pi/4)}{I(\beta = \pi/4) + I(\beta = -\pi/4)}. \quad (4)$$

Substituting Eq. (3) into Eq. (4), one can define the circular polarization in terms of θ , $\langle A_0 \rangle$ and $\langle O_0 \rangle$ as

$$P_c = \frac{\frac{\sqrt{15}}{2} \langle O_0 \rangle \cos \theta}{1 + \frac{5}{16} \langle A_0 \rangle (3 \cos^2 \theta - 1)}. \quad (5)$$

We present in Table I the calculated values of alignment and orientation in the $J=3/2$ level with σ^+ light (in our case), $J=1/2$ level with σ^+ and σ^- light, and $J=3/2$ level with σ^- light. Table also shows the calculated circular polarization values for the ${}^2S_{1/2} \rightarrow {}^2P_J \rightarrow {}^2S_{1/2}$ transition in the absence of depolarization effects. Thus, one can see that when $\theta=0$ the expected circular polarization degree is $P_c=1$ (100%), while for $\theta=\pi$, $P_c=-1$ (-100%).

TABLE I. The calculated values of alignment and orientation in the 2P_J level and circular polarization for the ${}^2S_{1/2} \rightarrow {}^2P_J \rightarrow {}^2S_{1/2}$ transition in the absence of depolarizing effects.

J	Excitation to J with σ^+ light			Excitation to J with σ^- light		
	$\langle A_0 \rangle$	$\langle O_0 \rangle$	P_c	$\langle A_0 \rangle$	$\langle O_0 \rangle$	P_c
1/2	0	$1/\sqrt{3}$	1	0	$-1/\sqrt{3}$	-1
3/2	2/5	$5/2\sqrt{15}$	1	2/5	$-5/2\sqrt{15}$	-1

IV. EXPERIMENTAL APPROACH

The schematic overview of the experimental apparatus is shown in Fig. 2. We used a pulsed neodymium-doped yttrium aluminum garnet (Nd:YAG) laser to pump two dye lasers which are directed colinearly into the interaction region of the Cs cell. The output from the second harmonic generator of the Nd:YAG laser produces light at 532 nm with an average power of 2 W using a pulse repetition rate of 20 Hz. The dye laser oscillators are constructed using a grazing-incidence Littman-Metcalf cavity and operate in a single transverse mode. Dye laser 1 is equipped with a dye circulating system to maintain the power stability around 0.03 mW, and it has a bandwidth of approximately 0.9 cm^{-1} . The output power of dye laser 2 from the oscillator is increased by about a factor of 10 using a dye amplification system which generates an average power of about 2 mW. Dye laser 2 has a bandwidth of approximately 0.2 cm^{-1} .

Two circularly polarized lasers are used to measure the circular polarization spectrum; the first circularly polarized light (dye laser 1) serves as the pump laser, and is used to excite the $6p^2P_{3/2}$ level at 852.1 nm. The second circularly polarized light (dye laser 2) is used to excite the final $10s^2S_{1/2}$ level at 603.4 nm. The wavelengths of the lasers are measured using a Coherent wavemeter with a precision of 0.001 nm. Both lasers are linearly polarized by using Glan-Thompson prism polarizers with extinction ratios of better than 10^{-5} . A high quality quarter-wave plate in the laser 1

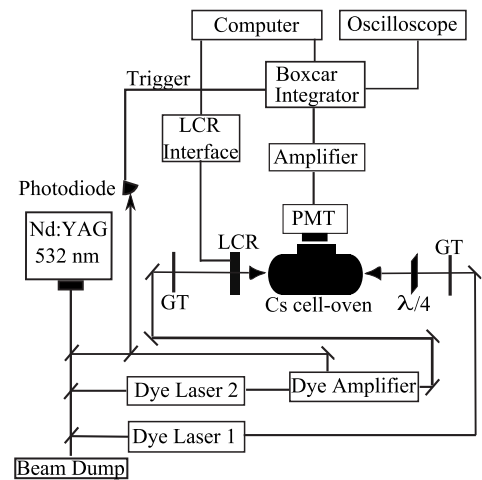


FIG. 2. A schematic diagram of the experimental apparatus. GT: Glan-Thompson prism polarizer; $\lambda/4$: quarter-wave plate; LCR: liquid-crystal variable retarder; PMT: photomultiplier tube.

beam path is used to produce circular polarization with positive helicity σ^+ . A temperature-controlled liquid crystal variable retarder (LCR) with an extinction ratio of 10^{-4} was used in the laser 2 beam path in order to alternately produce circular polarization with σ^+ and σ^- helicities. This was achieved by applying the necessary voltage to the retarder via a computer-controlled liquid crystal digital interface. Remote control of the experiment was managed using LabVIEW programming.

The sealed Pyrex cells containing Cs and up to 100 Torr Ar gas were prepared using an oil-free vacuum system and have 25.4 mm diameter by 50.8 mm length. The background pressure of the pure Cs cell is about 10^{-8} mbar. A resistively heated nonmagnetic cylindrical aluminum oven was used to hold the cells. The oven was wrapped with an aluminum oxide blanket to maintain the temperature better than ± 0.01 °C via a temperature controller.

The intensities of the cascade fluorescence from the $9p^2P_{1/2}$ level to the ground $6s^2S_{1/2}$ level were recorded at 361.73 nm by using a UV sensitive photomultiplier tube (PMT). The PMT was located at right angles to the propagation directions of the lasers. A combination of interference and color glass filters were used in front of the PMT in order to remove background due to scattered and atomic resonance fluorescence. The output of the PMT signal was sent to a boxcar with a 60 ns gate width which was opened after a 1 ns delay following the laser pulses. All the cables used in the experiment were electrically shielded and the optical table was grounded in order to eliminate electronic pickup and noise on the observed signal. The signals were digitized and stored on a computer while monitoring the size of the signal within the gate in real time using a digital oscilloscope operating at 500 MHz. Our typical signal size was about 10^3 photons for each laser pulse.

The ratio of the signals, detected when the helicities of the circularly polarized lasers are the same and opposite to each other generates a circular polarization degree, which may be experimentally determined as

$$P_c = \frac{S^{\sigma^+} - S^{\sigma^-}}{S^{\sigma^+} + S^{\sigma^-}}. \quad (6)$$

Equation (6) is the analog of Eq. (4), with the expressions S^{σ^+} and S^{σ^-} referring to the signals in each polarization channel; S^{σ^+} when the helicities of the lasers are $\sigma_1^+\sigma_2^+$ and S^{σ^-} when the helicities of the lasers are $\sigma_1^+\sigma_2^-$. In this expression, the labels 1 and 2 refer to laser 1 and laser 2. Some of the important transitions and their corresponding wavelengths [29,30] are illustrated in Fig. 3. An absolute intensity ratio of the signals is sensitive only to the relative polarization directions of the lasers. Therefore, any variations of the laser intensities with experimental factors such as absorbing medium density, fluorescence background, sensitivity of the gated boxcar integrator, collectively do not affect the intensity ratio.

V. RESULTS AND DISCUSSION

A. Depolarization due to hyperfine splitting in the absence of external perturbations

When an ensemble of atoms and molecules is aligned and oriented by an exciting laser field, the total electronic angular

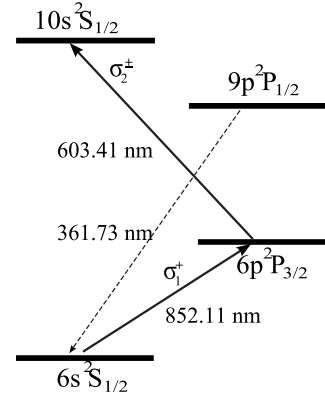


FIG. 3. Partial energy level diagram for atomic Cs, and an illustration of the experimental scheme. The dotted line shows the cascade fluorescence channel observed in the experiment.

momentum \vec{J} of the system stays fixed in space and quantized. For atoms with nonzero nuclear spin, the total angular momentum of the ensemble couples to the nuclear spin moment \vec{I} to produce a space-fixed \vec{F} , where \vec{F} is a total angular momentum. \vec{J} will then precess about \vec{F} so that the initially prepared space-fixed frame is altered. This precession affects all state multipoles. In the case of ^{133}Cs , the coupling of nuclear spin $I=7/2$ with $J=3/2$ introduces an oscillating time dependence in the alignment and orientation in the excited state. Therefore, the time evolution of the alignment and orientation under the influence of the hyperfine structure can be described as $\langle A_0(t) \rangle = \langle A_0 \rangle g^{(2)}(t)$ and $\langle O_0(t) \rangle = \langle O_0 \rangle g^{(1)}(t)$, respectively. Here, $g^{(k)}$ for $k=2$ and $k=1$ are the alignment and orientation hyperfine depolarization coefficients, respectively, and can be represented in the form [31,32]

$$g^{(k)}(t) = \sum_{F,F'} \frac{(2F+1)(2F'+1)}{(2I+1)} W^2(\xi) \cos(\omega_{FF'}t), \quad (7)$$

where $\omega_{FF'}$ is the frequency splitting between two hyperfine levels and $W(\xi) = W(JFJF'; Ik)$ is a Racah coefficient. Consequently, the circular polarization degree can be rewritten in terms of the alignment and orientation hyperfine depolarization coefficients [25] as

$$P_c = \frac{\sqrt{15} \langle O_0 \rangle g^{(1)}(t)}{2 + \frac{5}{4} \langle A_0 \rangle g^{(2)}(t)}. \quad (8)$$

The $g^{(2)}(t)$ and $g^{(1)}(t)$ coefficients decrease from their maximum value of 1 at $t=0$ and start to oscillate between the values of 1 and -1 as $t > 0$. This oscillation introduces time evolution in all state multipoles. However, if the temporal overlap time of the pulses can be made much less than the smallest hyperfine precession time ($T \ll 1/\omega_{FF'}$), one can possibly freeze out the electronic alignment and orientation in the excited level. That is, the atoms promoted to the final level by the two-photon excitation emit the photons before the hyperfine precessional motion can be taken place. The overlap time of our pulse lasers (~ 1.1 ns) and the smallest hyperfine precession in the excited level are comparable.

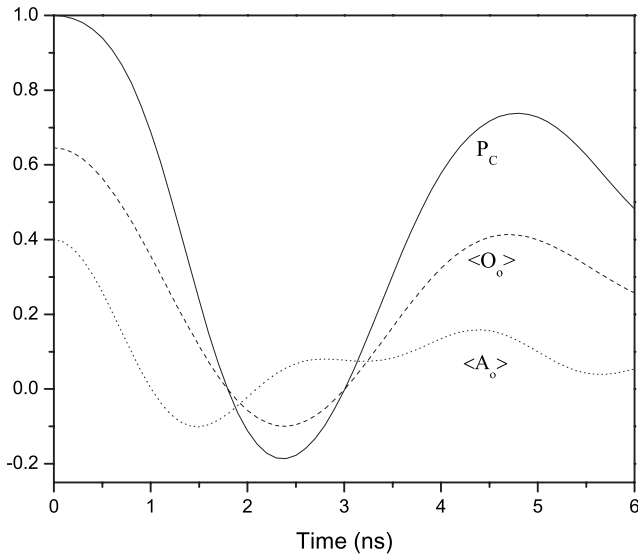


FIG. 4. Time evolution of alignment (dotted line), orientation (dashed line), and circular polarization (solid line).

Thus, all state multipoles are expected to be perturbed by the hyperfine interaction which in return decreases the circular polarization degree. Figure 4 illustrates the theoretical time evolution of the alignment and circular polarization over 6 ns. For example, at the 1.1 ns overlap time, theory shows that $g^{(2)} = -0.08$ and $g^{(1)} = 0.47$ and thus polarization is expected to be reduced from 1 to 0.6 within 1.1 ns. The measured circular polarization degree for the $6s^2S_{1/2} \rightarrow 10s^2S_{1/2}$ transition is found to be 59.8(2)%. This yields the value of $g^{(2)} = -0.0892(44)$ and $g^{(1)} = 0.4764(34)$ which show a good agreement with the theory [22].

B. External perturbations on the polarization spectrum

We have also checked for the existence of external perturbations such as radiation trapping, collisional ionization, and the influence of laser power. Due to the short temporal overlap time of the pulses compared to the radiative lifetime of the excited level ($\tau = 33$ ns), approximately 3% of the excited atoms will have radiatively decayed during the pulse. Therefore, we expected radiation trapping has a negligible effect on the excited level. In order to be assure that the laser powers and Cs cell temperature were not modifying the measured polarization degree during the two-photon on-resonant excitation, measurements of laser power and temperature dependence to the polarization spectra were performed separately. Both results were found to be independent of laser power and Cs density. Other external perturbations may be involved in an optically thick medium such as collisional ionization. Several authors have experimentally studied the collisional ionization of highly excited level alkali metal at high temperatures [8,33,34]. Systematic measurements in such studies show that the associative ionization rate constants (k_{AI}) is $5 \times 10^{-10} \text{ cm}^3 \text{ s}^{-1}$ for Rb ($8s, 7d$) and $0.5 \times 10^{-9} \text{ cm}^3 \text{ s}^{-1}$ for Na ($17 < n < 27, l=0, 1, 2$). Comparison of these ionization rate constants against the effective quantum number yields rough upper and lower limits for our Cs cell condition. Since

the ionization rate is small compared with the radiative decay rate of the final level, our system is essentially free of collisional ionization.

The dynamical interaction of the electronic and nuclear spins in the excitation and cascade fluorescence sequences of the experiments we describe here are generally complicated. The most important of these occurs in the resonantly excited $6p^2P_{3/2}$ level; this has been discussed elsewhere in this report. However, it is generally possible that electronic-nuclear spin dynamics can alter the relative intensities measured (in the $9p$ - $6s$ channel) for the two different circular polarization excitation geometries used here. For example, if the optical excitation generates an electronic orientation in the $10s$ level, that orientation couples to the partially polarized nuclear spin, modifying both during the 265 ns lifetime [35] of the $10s$ level. In addition, following cascade to the $9p$ multiplet levels a similar hyperfine structure mediated dynamics also occurs. Overall, the measured fluorescence intensities can complexly depend on the orientation dynamics in the atomic system [36,37]. However, the present experiment was designed to minimize such effects. This was accomplished by defining the orientation axis to be along the pump and probe laser propagation directions (the helicity axis), and by selecting a detector location at 90° to this direction. It can be shown that, for this geometry, the fluorescence intensity in a generally oriented system does not depend on the numerical value of the orientation [25]. In the context of this report, this ensures that the measured fluorescence intensities are sensitive only to the relative populations generated in the $10s$ level for the two circular polarization channels.

In the absence of any depolarizing effects, circular polarization P_c is 1. However, we expect $P_c = 0.6$ when nuclear spin and total angular momentum coupling is considered with no other systematic errors. Hence, our circular polarization spectra obtained for the $6s^2S_{1/2} \rightarrow 10s^2S_{1/2}$ transition confirm that $J=3/2$ level has no external perturbations that measurably alter the alignment and orientation in the $6p^2P_{3/2}$ level. Consequently, both alignment and orientation hyperfine depolarization coefficients at $T=1.1$ ns were taken into account in order to treat for the depolarizing influence of the unobserved hyperfine interaction.

C. Rate equation analysis of Zeeman populations

The variety of possible distributions of atoms in the Zeeman magnetic sublevels depends on the given experimental conditions such as optical pumping with a circularly or linearly polarized light source. In our experiment, the selective excitation to the Zeeman magnetic sublevels of the $6p^2P_{3/2}$ level was done using a circularly polarized laser light source. In the presence of Ar atoms, collisions between the excited Cs atoms (in the $m=3/2$ and $m=1/2$ sublevels) and the ground-level argon atoms redistribute the population in the Zeeman sublevels, and thus transfer population between different magnetic sublevels. The population ($N_{\pm 1/2}$, $N_{\pm 3/2}$) mixing among the $m = \pm 1/2, \pm 3/2$ magnetic sublevels is responsible for the reduction of the alignment and orientation produced in the excited level. The collisional mixing processes are illustrated in Fig. 5. Note that all collisional mix-

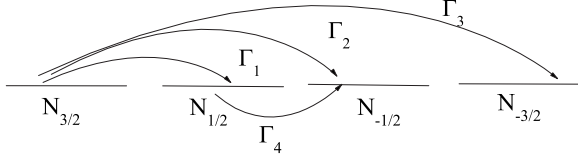


FIG. 5. Population mixing among the Zeeman sublevels of the $6p^2P_{3/2}$ level cesium atoms.

ing possibilities are bidirectional with equal rates. The population variations among the Zeeman sublevels of the $6p^2P_{3/2}$ level due to collisions with argon gas can be expressed by a simple theoretical model using rate equation analysis of Zeeman populations. The rate of change of population in each magnetic sublevel can be written as

$$\begin{aligned}\dot{N}_{3/2} &= -\Gamma_{32}N_{3/2} + \Gamma_1N_{1/2} + \Gamma_2N_{-1/2} + \Gamma_3N_{-3/2} + \Gamma_p, \\ \dot{N}_{1/2} &= -\Gamma_{12}N_{1/2} + \Gamma_4N_{-1/2} + \Gamma_2N_{-3/2} + \Gamma_1N_{3/2} + \Gamma'_p, \\ \dot{N}_{-1/2} &= -\Gamma_{12}N_{-1/2} + \Gamma_4N_{1/2} + \Gamma_2N_{3/2} + \Gamma_1N_{-3/2}, \\ \dot{N}_{-3/2} &= -\Gamma_{32}N_{-3/2} + \Gamma_1N_{-1/2} + \Gamma_2N_{1/2} + \Gamma_3N_{3/2},\end{aligned}\quad (9)$$

where $\Gamma_{12}=(\gamma+\Gamma_1+\Gamma_2+\Gamma_4)$ and $\Gamma_{32}=(\gamma+\Gamma_1+\Gamma_2+\Gamma_3)$, and γ is the radiative decay rate and, $\Gamma_{1,2,3,4}$ are the collision-induced transition decay rates. For excitation with a positive photon helicity, Γ_p and Γ'_p indicate the relative pump rates to the $m=3/2$ and $m=1/2$, respectively. Since these pump rates depend on the squared Clebsch Gordon coefficients, one can calculate the ratio of the pump rates involved in the polarization measurement. The net rate of change of the total density N , alignment $\langle A_0(t) \rangle$ and orientation $\langle O_0(t) \rangle$ in the excited level can be written as

$$\dot{N}(t) = -\gamma N + (\Gamma_p + \Gamma'_p), \quad (10a)$$

$$\langle \dot{A}_0(t) \rangle = -\gamma_a \langle A_0(t) \rangle + 4(\Gamma_p - \Gamma'_p)/5, \quad (10b)$$

$$\langle \dot{O}_0(t) \rangle = -\gamma_0 \langle O_0(t) \rangle + (3\Gamma_p + \Gamma'_p)/\sqrt{15}, \quad (10c)$$

where $\gamma_a = \gamma + (2\Gamma_1 + 2\Gamma_2)$ and $\gamma_0 = \gamma + (-2\Gamma_1 + 4\Gamma_2 + 2\Gamma_4)$ are the alignment and orientation decay rates, respectively. Here, $\Gamma_a = (2\Gamma_1 + 2\Gamma_2)$ and $\Gamma_0 = (-2\Gamma_1 + 4\Gamma_2 + 2\Gamma_4)$ are responsible for the collisional mixing and contain information about the gas-kinetic cross section relations. The time-dependent solutions of the Eqs. (10) in the excited level can be derived as

$$N(t) = \frac{(\Gamma_p + \Gamma'_p)}{\gamma} (1 - e^{-\gamma t}), \quad (11a)$$

$$\langle A_0(t) \rangle = \frac{4(\Gamma_p - \Gamma'_p)}{\gamma_a} (1 - e^{-\gamma_a t}), \quad (11b)$$

$$\langle O_0(t) \rangle = \frac{(3\Gamma_p + \Gamma'_p)}{\sqrt{15}\gamma_0} (1 - e^{-\gamma_0 t}). \quad (11c)$$

Note that the steady-state value of the total population density N at $t=\infty$ is $(\Gamma_p + \Gamma'_p)/\gamma$. We assumed that the total population density is zero at $t=0$. We can define the population in each Zeeman sublevel in terms of the monopole, dipole and quadrupole components of the total density for the $J=3/2$ atoms as

$$N_{3/2}(t) = \frac{1}{4}N(t) + \frac{5}{16}\langle A_0(t) \rangle + \frac{3\sqrt{15}}{20}\langle O_0(t) \rangle, \quad (12a)$$

$$N_{1/2}(t) = \frac{1}{4}N(t) - \frac{5}{16}\langle A_0(t) \rangle + \frac{\sqrt{15}}{20}\langle O_0(t) \rangle, \quad (12b)$$

$$N_{-1/2}(t) = \frac{1}{4}N(t) - \frac{5}{16}\langle A_0(t) \rangle - \frac{\sqrt{15}}{20}\langle O_0(t) \rangle, \quad (12c)$$

$$N_{-3/2}(t) = \frac{1}{4}N(t) + \frac{5}{16}\langle A_0(t) \rangle - \frac{3\sqrt{15}}{20}\langle O_0(t) \rangle. \quad (12d)$$

The measured signals, integrated over the temporal overlap time of the pulses, can be defined as

$$S^{\sigma^+} = \frac{3}{4} \int_0^T N_{-3/2} dt + \frac{1}{4} \int_0^T N_{-1/2} dt, \quad (13a)$$

and

$$S^{\sigma^-} = \frac{3}{4} \int_0^T N_{3/2} dt + \frac{1}{4} \int_0^T N_{1/2} dt. \quad (13b)$$

Substituting Eqs. (12) into (13a) and (13b), we can express the circular polarization degree in terms of argon pressure as

$$P_c(p) = \frac{S^{\sigma^+} - S^{\sigma^-}}{S^{\sigma^+} + S^{\sigma^-}} = \frac{5Z_0}{4 + Z_a}, \quad (14)$$

where

$$Z_a = \frac{\gamma g^{(2)}(t)}{\gamma_a} \left\{ \frac{1 + \frac{1}{\gamma_a T} (e^{-\gamma_a T} - 1)}{1 + \frac{1}{\gamma T} (e^{-\gamma T} - 1)} \right\}, \quad (15a)$$

and

$$Z_0 = \frac{\gamma g^{(1)}(t)}{\gamma_0} \left\{ \frac{1 + \frac{1}{\gamma_0 T} (e^{-\gamma_0 T} - 1)}{1 + \frac{1}{\gamma T} (e^{-\gamma T} - 1)} \right\}. \quad (15b)$$

In Eqs. (15a) and (15b), $\gamma_a = \gamma + \Gamma_a$ and $\gamma_0 = \gamma + \Gamma_0$ are defined. The disalignment and disorientation cross sections σ_a and σ_0 , respectively, may be defined using gas-kinetic cross section relations as

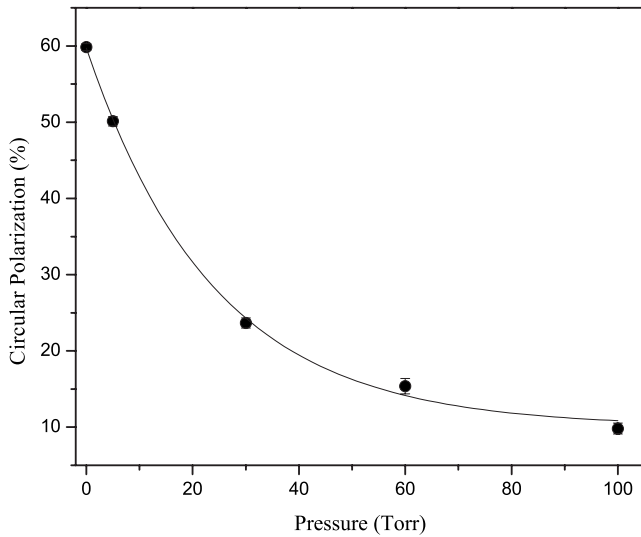


FIG. 6. Nonlinear least square fit of the circular polarization spectrum for the 6S-10S transition.

$$\Gamma_0 = \frac{p}{kT} \sigma_0 \bar{v}_{\text{CsAr}},$$

and

$$\Gamma_a = \frac{p}{kT} \sigma_a \bar{v}_{\text{CsAr}},$$

where p is the buffer gas pressure, k is the Boltzmann's constant, and T is the average cell temperature. Thus, Eq. (14) provides the connection between the experimentally measured circular polarization degree P_c and the disorientation cross section σ_0 . We assume that $\langle \sigma_0 v \rangle$ may be factored so that $\langle v \rangle$ can be written as \bar{v}_{CsAr} which is the average velocities of the colliding Cs-Ar atoms over the Maxwell-Boltzmann distribution of relative velocities at the cell temperature.

In order to extract the disorientation cross section from the measured circular polarization spectra at argon gas pressures ranging from 5 to 100 Torr, we used the experimentally measured disalignment cross section found from our earlier work [38]. Rate equation analysis of the $6p^2P_{3/2}$ level population was made assuming the laser pulse temporal profile as rectangular pulse and the pulse width was measured to be approximately 6.5 ns using a 0.2-ns rise-time ultrafast photodetector. The result of the nonlinear least-squares fit to the data is illustrated in Fig. 6. The error bars indicate one standard deviation. The disorientation cross section value, extracted from the nonlinear-least square fit of the experimental results, is in good agreement with the theoretical [20]

TABLE II. Disalignment (σ_a) and disorientation (σ_0) cross sections of the $6p^2P_{3/2}$ level cesium atoms independent of nuclear-spin effect are listed.

$\sigma_0(\text{\AA}^2)$	σ_a/σ_0	References
151(42)	1.23(4)	This work ^a
192		[20]
234(34)	1.23(18)	[17] ^b
188(38)		[18] ^c

^aTwo-photon pulse laser technique using circular polarization.

^bZeeman scanning technique at 5.3 kG.

^cOptical pumping technique.

and experimental [17,18] values, as seen by the summary in Table II. The disorientation cross sections measured using Zeeman scanning technique at 5.3 kG in Ref. [17] and $D2$ optical pumping technique in Ref. [18] are not significantly different from those yielded by this work within experimental error. Although different models were used to interpret the optical pumping results [18], we listed the data from the J -randomization model for comparison. The ratio σ_a/σ_0 is predicted to be in between 1.5 and 3 for the collisions with Ar [17,39] but 1 for the collisions with lighter gases. Thus, the investigation of the disalignment and disorientation cross sections in the $6p^2P_{3/2}$ level Cs atoms in collisions with lighter gases such as Kr and He using two-photon two-color pulse laser technique is currently underway.

VI. CONCLUSIONS

We have measured circular polarization spectra of the two-photon two-color double-resonance $6s^2S_{1/2} \rightarrow 6p^2P_{3/2} \rightarrow 10s^2S_{1/2}$ transition as a function of Ar gas pressure up to 100 Torr. The theoretical evolution of the alignment and orientation, in the presence of hyperfine precession for $J=3/2$ cesium atoms, has a good agreement with the measured value at $T=1.1$ ns. The spectra were found to be independent of external perturbations. From the measured circular polarization spectra, we extracted the disorientation cross section which is in good agreement with the experiment and theoretical predictions within error limits. We used two-photon pulse laser technique and defined the circular polarization degree in terms of alignment, orientation, and argon gas pressure.

ACKNOWLEDGMENTS

We acknowledge support from the Research Corporation under Grant No. CC7133.

- [1] L. Cook, D. Olsgaard, M. D. Havey, and A. Sieradzan, *Phys. Rev. A* **47**, 340 (1993).
- [2] R. A. Lasell, B. S. Bayram, M. D. Havey, D. V. Kupriyanov, and S. V. Subbotin, *Phys. Rev. A* **56**, 2095 (1997).
- [3] T. H. Wong and P. D. Kleiber, *Phys. Rev. A* **57**, 2227 (1998).
- [4] L. B. Zhao, A. Watanabe, P. C. Stancil, and M. Kimura, *Phys. Rev. A* **76**, 022701 (2007).
- [5] C. Y. Lin, P. C. Stancil, Y. Li, J. P. Gu, H. P. Liebermann, R. J. Buenker, and M. Kimura, *Phys. Rev. A* **76**, 012702 (2007).
- [6] J. Weiner, V. S. Bagnato, S. Zilio, and P. S. Julienne, *Rev. Mod. Phys.* **71**, 1 (1999).
- [7] D. Leibfried, R. Blatt, C. Monroe, and D. Wineland, *Rev. Mod. Phys.* **75**, 281 (2003).
- [8] T. F. Gallagher, *Rydberg Atoms* (Cambridge University Press, Cambridge, 1994).
- [9] A. Walz-Flannigan, J. R. Guest, J.-H. Choi, and G. Raithel, *Phys. Rev. A* **69**, 063405 (2004).
- [10] K. R. Overstreet, A. Schwettmann, J. Tallant, and J. P. Shaffer, *Phys. Rev. A* **76**, 011403(R) (2007).
- [11] C. I. Sukenik, D. Hoffmann, S. Bali, and T. Walker, *Phys. Rev. Lett.* **81**, 782 (1998).
- [12] W. C. Stwalley and H. Wang, *J. Mol. Spectrosc.* **195**, 194 (1999).
- [13] J. P. Shaffer, W. Chalupczak, and N. P. Bigelow, *Phys. Rev. Lett.* **83**, 3621 (1999).
- [14] C. I. Sukenik and H. C. Busch, *Phys. Rev. A* **66**, 051402(R) (2002).
- [15] A. Derevianko, S. G. Porsev, S. Kotochigova, E. Tiesinga, and P. S. Julienne, *Phys. Rev. Lett.* **90**, 063002 (2003).
- [16] K. M. Jones, E. Tiesinga, P. Lett, and P. S. Julienne, *Rep. Prog. Phys.* **78**, 483 (2006).
- [17] J. Guiry and L. Krause, *Phys. Rev. A* **14**, 2034 (1976).
- [18] J. Fricke, J. Haas, and E. Lüscher, *Phys. Rev.* **163**, 45 (1967).
- [19] B. R. Bulos and W. Happer, *Phys. Rev. A* **4**, 849 (1971).
- [20] A. I. Okunevich and V. I. Perel, *Sov. Phys. JETP* **31**, 356 (1970).
- [21] W. E. Baylis, *Progress in Atomic Spectroscopy* (Plenum, New York, 1978), Pt. B, Chap. 28.
- [22] K. Blum, *Density Matrix Theory and Applications* (Plenum, New York, 1981).
- [23] R. N. Zare, *Angular Momentum* (Wiley, New York, 1988).
- [24] M. D. Havey (private communication).
- [25] C. H. Greene and R. N. Zare, *Annu. Rev. Phys. Chem.* **33**, 119 (1982).
- [26] K. B. MacAdam and M. A. Morrison, *Phys. Rev. A* **48**, 1345 (1993).
- [27] U. Fano and J. H. Macek, *Rev. Mod. Phys.* **45**, 553 (1973).
- [28] M. E. Rose, *Elementary Theory of Angular Momentum* (Wiley, New York, 1957).
- [29] A. A. Radzig and B. M. Smirnov, *Reference Data on Atoms, Molecules, and Ions* (Springer-Verlag, New York, 1985).
- [30] K.-H. Weber and C. J. Sansonetti, *Phys. Rev. A* **35**, 4650 (1987).
- [31] E. Arimondo, M. Inguscio, and P. Violino, *Rev. Mod. Phys.* **49**, 31 (1977).
- [32] N. Andersen and K. Bartschat, *Polarization, Alignment, and Orientation in Atomic Collisions* (Springer-Verlag, New York, 2001).
- [33] J. Weiner and J. Boulmer, *J. Phys. B* **19**, 599 (1986).
- [34] M. Cheret, L. Barbier, W. Lindinger, and R. Deloche, *J. Phys. B* **15**, 3463 (1982).
- [35] W. S. Neil and J. B. Atkinson, *J. Phys. B* **17**, 693 (1984).
- [36] A. Sieradzan, J. Krasinski, and F. A. Franz, *J. Phys. B* **16**, 43 (1983).
- [37] T. R. Marshall, R. Boggy, and F. A. Franz, *Phys. Rev. A* **16**, 618 (1977).
- [38] S. B. Bayram, S. Kin, M. J. Welsh, and J. D. Hinkle, *Phys. Rev. A* **73**, 042713 (2006).
- [39] W. Berdowski, T. Shiner, and L. Krause, *Phys. Rev. A* **4**, 984 (1971).